Meehl Gerald, A. (Orcid ID: 0000-0002-8760-9534)

Arblaster Julie, M. (Orcid ID: 0000-0002-4287-2363)

Rosenbloom Nan, A. (Orcid ID: 0000-0001-7389-3346)

Neale Richard (Orcid ID: 0000-0003-4222-3918)

Lauritzen Peter, Hjort (Orcid ID: 0000-0001-7066-138X)

Bryan Frank, O. (Orcid ID: 0000-0003-1672-8330)

Hannay Cecile (Orcid ID: 0000-0001-6363-6151)

Shields Christine, A (Orcid ID: 0000-0003-4481-1377)

Strand Warren, G (Orcid ID: 0000-0001-9740-0104)

Danabasoglu Gokhan (Orcid ID: 0000-0003-4676-2732)

Effects of model resolution, physics, and coupling on Southern Hemisphere storm tracks in CESM1.3

Gerald A. Meehl[1*], Dongxia Yang[2], Julie M. Arblaster[1,2], Susan C. Bates[1], Nan Rosenbloom[1], Richard Neale[1], Julio Bacmeister[1], Peter H. Lauritzen[1], Frank Bryan[1], Justin Small[1], John Truesdale[1], Cecile Hannay[1], Christine Shields[1], Warren G. Strand[1], John Dennis[1], and Gokhan Danabasoglu[1]

1. National Center for Atmospheric Research, Boulder, CO, USA
2. ARC Centre of Excellence for Climate Extremes, Monash University, Melbourne, Australia

This article has been accepted for publication and undergone full peer review but has not been through the copyediting, typesetting, pagination and proofreading process which may lead to differences between this version and the Version of Record. Please cite this article as doi: 10.1029/2019GL084057

September 8, 2019

*Corresponding author: Gerald A. Meehl
National Center for Atmospheric Research
PO Box 3000
Boulder, CO 80307
meehl@ucar.edu
ORCID: 0000-0002-8760-9534

Key points:

--Progression from CESM1.1 to CESM1.3 is documented with improved physics and better simulation of low clouds in CESM1.3 compared to CESM1.1

--Southern Hemisphere storm tracks intensify in closer agreement with observations with higher resolution in the atmosphere except in the model version with older physics

--Deficient physics in the atmospheric model can negate the gains attained by higher resolution in atmosphere and ocean.

Plain language summary: Southern Hemisphere storm tracks intensify in closer agreement with observations with higher resolution in the atmosphere except in the model version with older physics, such that deficient physics in the atmospheric model, which produce less low clouds, a reduced meridional SST gradient, and weaker storms in the Southern Hemisphere, can negate the gains attained by higher resolution in atmosphere and ocean.

Two high-resolution versions of a coupled Earth system model (CESM1.3: 0.25˚-atmosphere, 1˚-ocean; CESM1.1: 0.25˚-atmosphere, 0.1˚-ocean) are compared to the standard resolution CESM1.1 and CESM1.3 (1˚-atmosphere, 1˚-ocean). The CESM1.3 versions are documented, and the consequences of model resolution, air-sea coupling, and physics in the atmospheric models are studied with regards to storm tracks in the Southern Hemisphere as represented by 850 hPa eddy kinetic energy. Increasing the resolution from 1˚ to 0.25˚ in the atmosphere (same physics) coupled to the 1˚-ocean intensifies the strength of the storm tracks closer to observations. The 0.25˚-atmosphere with the older CESM1.1 physics coupled to the 0.1˚-ocean has fewer low clouds, warmer

Southern Ocean SSTs, a weaker meridional temperature gradient, and a degraded storm track simulation compared to the 0.25°-atmosphere with CESM1.3 physics coupled to the 1°-ocean. Therefore, deficient physics in the atmospheric model can negate the gains attained by higher resolution in atmosphere and ocean.

1. Introduction

There is extensive literature documenting the benefits of higher horizontal resolution in an atmospheric model for better simulating atmospheric dynamics (e.g. Shaffrey et al., 2009; Hertwig et al., 2015; Roberts et al., 2018). In most cases, improvements in atmospheric model resolution are implemented in models with either the same physics or improved physics as successive generations of models typically evolve with joint advances in both resolution and physics. Therefore, it is usually assumed that higher horizontal resolution will produce better simulations of midlatitude storm systems, and thus improved representations of storm tracks (Hertwig et al., 2015). Other factors can contribute to improved simulations of storm tracks, such as warmer base-state midlatitude sea surface temperatures (SSTs) that have been shown to produce better-simulated storm tracks in different ocean model resolutions with the same atmospheric model resolution (Small et al., 2018).

Here we study historical simulations with variants of the Community Earth System Model version 1 (CESM1) that evolved from CESM1.1 to CESM1.3, and provide documentation of these various model configurations that involve different atmospheric model resolutions, with different convection and cloud physics formulations, coupled to different ocean model resolutions. Though some limited CESM1.3 results have appeared in the literature before (e.g. Baker et al., 2015), this paper represents the first detailed documentation of CESM1.3.

The goal is to identify the combination of model resolution and physics that can produce an improved simulation of Southern Hemisphere midlatitude storm tracks.

The seasonal cycle of storm tracks in the Southern Hemisphere is weaker than their Northern Hemisphere counterparts, but not negligible (Trenberth 1991). The summer is marked by a single atmospheric jet stream and a narrowly confined storm track, whilst the winter exhibits a sub-tropical jet and polar-front jet with most of the near-surface storm track activity associated with the latter (Trenberth 1991, Nakamura and Shimpo 2004) but it is broader in latitudinal extent than summer. Here we focus on Southern Hemisphere winter.

There is a marked zonal asymmetry with stronger storm tracks in the Atlantic and Indian Ocean than in the Pacific (Trenberth 1991, Hoskins and Hodges 2005) and previous work has shown that the zonal structure is sensitive to both tropical SST and teleconnections, as well as midlatitude SST gradients (Inatsu and Hoskins 2004). Furthermore, the atmospheric jet stream and low cloud cover are related (Grise and Polvani 2014, Bony et al. 2015, Ceppi and Hartmann 2015). For example, cloud shortwave forcing can produce changes in surface energy balance and meridional SST gradients that can affect baroclinicity and the consequent strength of the jet stream (Ceppi et al., 2012). Thus, simulating Southern Hemisphere storm tracks is a strong test of a model in that it has to reasonably represent large-scale dynamics as well as low clouds and SST gradients.

Here we hypothesize that the model with older physics, which produces less low clouds, will simulate a reduced meridional SST gradient across the Southern Ocean with reduced baroclinicity and a weaker storm track in spite of having higher resolution that could contribute to a stronger storm track.

2. Documentation of model configurations

Versions of the CESM1 (Hurrell et al. 2013) analyzed here use the CAM5 atmospheric model (Park et al., 2014) with finite volume (FV, used in the CESM1.1 large ensemble version, Kay et al., 2015) and spectral element (SE, in CESM1.3 versions) dynamical cores (Dennis et al. 2012). Other components are the Community Ice Code version 4 for sea ice (CICE4, Hunke and Lipscomb 2008), the Parallel Ocean Program version 2 for the ocean (POP2, Smith et al. 2010, Danabasoglu et al. 2011), and the Community Land Model version 4 (CLM4, Lawrence et al. 2011) with the River Transport Model version 1 (RTM1).

As summarized in Meehl et al. (2013 and references therein), CAM5 in these CESM1 versions added a number of new advances from its predecessor CAM4, including a new boundary layer, shallow convection, radiation and microphysics schemes, as well as fully interactive aerosols. Amongst the features seen in CAM5 simulations are improved representations of cloud properties such as total cloud amount, optically thick cloud amount, and midlevel cloud (e.g. Kay et al. 2012, Medeiros et al. 2012), as well as reduced resolution dependence of certain fields such as short and long –wave cloud forcing (Bacmeister et al. 2014).

In the simulations analyzed here, CAM5 has a horizontal resolution of either 1.0 º or 0.25º and the standard 30 levels in the vertical, with a model top of 3hPa. The POP2 model has a nominal grid spacing of either 1.0 º or 0.1º. The 1.0° resolution version has a displaced North Pole over Greenland and refinement at the equator of approximately 30km in latitude and 125km in longitude. The 0.1° version of POP2 uses a tripole grid with two poles in the

Northern Hemisphere over North America and Asia and horizontal resolution decreasing from 11km at the equator to 2.5km at high latitudes. The 0.1° ocean configuration is similar to that used in McClean et al. (2011) and Kirtman et al. (2012). The 0.1° ocean model uses partial cell topography (Adcroft et al, 1997) with a maximum depth of 6000m (62 levels), while the 1° ocean model uses full cell topography with a maximum depth of 5500m (60 levels). The land and sea ice models are run at the same resolution and grid as the atmosphere and ocean models respectively.

The various coupled models are shown in Table 1 and are described here. The fully-coupled CESM1.3 simulations using the 1° and 0.25° versions of CAM5 with the SE dynamical core coupled to the 1° ocean/sea-ice (hereafter '1x1_v1.3' with three ensemble members; and '0.25x1_v1.3' with two ensemble members, respectively) were conducted with the CESM1.3 beta 17 model version. Experiments with this version were designed to perform higher resolution atmospheric simulations with improved model physics. Note that a new version of the SE dycore in CESM2 (not used here) has several improvements for high resolution applications such as a dry-mass vertical coordinate, condensate loading, rigorous energy formulation that includes condensates and much improved viscosity (Lauritzen et al., 2019).

CESM1.1 fully-coupled simulations with the FV dynamical core in CAM5 with ocean and sea ice at 1° (hereafter '1x1_v1.1') were those produced for the CESM1 Large Ensemble (Kay et al. 2015). We analyze 42 members from this ensemble. Subsampling this large ensemble with a smaller number of ensemble members closer to the ensemble size of the other simulations in the present paper produces similar results as shown the Supplementary Information. All of these model experiments incorporate time varying natural and anthropogenic historical forcings (see Meehl et al. 2012, and Meehl et al 2013 for details) and

are analyzed for the years 1979-2005 to focus on the recent period for which reanalysis products are better constrained with satellite observations over the Southern Ocean. Note the ozone forcing differs in the 1x1_v1.1 run but has little impact in the winter season. Simulations with the CESM1.1 with the older physics use a 0.25° version of CAM5 with the SE dynamical core coupled to a 0.1° resolution ocean/sea-ice (hereafter '0.25x0.1_v1.1', documented in Small et al., 2014). This present-day control (constant year-2000 conditions) was run for 100 years. As noted in Small et al (2014), "present-day" (year 2000) greenhouse gas condition (fixed CO2 concentration of 367 ppm) was chosen to facilitate direct comparisons with recent-era observations. There were 10 years of daily data saved from that run and are analyzed here. While internal decadal variability could play a factor in influencing the results if a greater number of years was available for analysis, and this is certainly a caveat that must accompany these results, the AMIP experiments for longer averaging periods (discussed below in Fig. 1) indicate similar results with the older physics in the amip_0.25d_v1.1 compared to the newer physics in the CESM1.3 version amip_0.25d_v1.3. A subsequent extension of the original Small et al (2014) simulation for years 2001-2015 where daily data was saved (Fig. S3) shows very similar results to the constant year-2000 run in Fig. 1d. Additionally, the processes and mechanisms invoked below indicate physical consistency across the different model resolutions and versions.

We also conducted three atmosphere/land-only AMIP-style experiments with observed time-evolving SSTs from 1979-2005 (where AMIP denotes Atmospheric Model Intercomparison Project, typically an atmospheric model run with observed SSTs). The observed SSTs (also used in Fig. 2c) are 1° resolution from Hurrell et al (2008) and can be found at https://climatedataguide.ucar.edu/climate-data/merged-hadley-noaaoi-sea-surface-temperature-sea-ice-concentration-hurrell-et-al-2008. In the 0.25° atmosphere versions, the

surface fluxes are calculated on the atmospheric model grid (Zarzycki et al., 2016). All of these were conducted with the SE-dycore. One used the CESM1.3 version at 1° resolution ('amip_1d_v1.3'), another the CESM1.3 version at 0.25° resolution ('amip_0.25d_v1.3'), and the third used the CESM1.1 at 0.25° resolution ('amip_0.25d_v1.1'). As shown in Table 1, the 'amip_1d_v1.3' is the AMIP version of 1x1_v1.3 for direct comparison with the coupled run and to test the influence of the air-sea coupling. The 'amip_0.25d_v1.3' is the AMIP version of 0.25x1_v1.3 but uses an earlier version specifically called CESM1.3 beta 02, and 'amip_0.25d_v1.1' is the AMIP version of 0.25x0.1_v1.1.

The evolution from CESM1.1 to CESM1.3 included a CESM1.2 version (e.g. Tilmes et al., 2015; Brady et al., 2019):

http://www.cesm.ucar.edu/models/cesm1.2/tags/index.html#CESM1_2_2_1.

From versions of CESM1.1 that had both the FV and SE dycores, the progression from CESM1.1 to CESM1.2 (and also in CESM1.3) involved a change from Eulerian to Lagrangian vertical advection within the SE-dycore that increased low clouds in better agreement with observations. Then progressing from CESM1.2 to the CESM1.3 development series (e.g. some results shown in Baker et al., 2015, with no model description), there are five notable changes. The first is a minor microphysics rearrangement changing the order of operations relating to cloud and atmospheric water content as well as a bug fix to the microphysics code. The second occurred within the radiation code (RRTMG) in which there was a fix in the calculation of radiation to reduce spikes in surface temperature that occasionally occurred at a few grid points. This was not a climate-changing effect unless very high temperatures occurred. Third and fourth were updates to the heterogeneous freezing code and a new gravity wave scheme, respectively. Finally, throughout the CESM1.3 development series, there were changes to dust tuning and soil erodibility. Though a new land

model, CLM4.5, was an option in the CESM1.2 and CESM1.3 model versions, the CLM4 land model is used in all of simulations considered here. The CESM1.3 model code can be obtained at http://www.cesm.ucar.edu/experiments/ with permission from the CESM Chief Scientist.

Using AMIP simulations simulating the present day period used within this study (1979-2004) for each incremental model version, we find that the most impactful developments are the changes to vertical advection, the gravity wave scheme, dust parameterization, and changing from the FV to the SE dycore. The largest improvements in the model's representation of clouds and the position of the Southern Hemisphere jet occur in the upgrade from FV to SE and with the changes in vertical advection (occurring between the CESM1.1 and CESM1.2 versions). The change associated with the microphysics (occurring between CESM1.3 beta 02 and beta 17) appears to have degraded the representation of high clouds in the northern hemisphere midlatitudes as well as low clouds at all latitudes. Though degraded from the CESM1.3 beta 02 representation, the results are still a large improvement over the CESM1.1 code using the FV dycore.

The major outcome of the physics changes in the CESM1.3 beta 17 version compared to the other versions of CESM1.1 and CESM1.2 is that the high and low cloud simulation is improved, with general increases in low cloud in CESM1.3 in better agreement with observations. This change in low clouds will prove to be important in the analyses below.

We represent storm tracks here as 850 hPa eddy kinetic energy (Maloney, 2009) as given by:

$$EKE = (U'^2 + V'^2)/2$$

where the prime represents the 2.5-6 days bandpass filter.

3. Results

a. Storm tracks and meridional temperature gradient

The storm tracks for JJA represented by the 850 hPa EKE in ERA-Interim reanalysis (Fig. 1e) are strong in the midlatitude Atlantic Ocean and Indian Oceans, and weaker in the Pacific Ocean as noted above (e.g. Hoskins and Hodges 2005). The storm track EKE maxima in the southeast Pacific is centered near 45˚S, and in the southern Atlantic/Indian Oceans at about 55˚S, indicating more influence of the subtropical jet in the former basin and subpolar jets in the latter (Nakamura and Shimpo 2004). Looking in more detail, the strongest EKE is south and east of South Africa and there is a secondary maximum off Antarctica at around the dateline. The growth of storms in the Atlantic and Indian Ocean is generally attributed to cyclogenesis in the lee of the Andes, followed by some strengthening by meridional SST gradients (Hoskins and Hodges 2005, Nakamura and Shimpo 2004). The local maximum off Antartica (~180°, near Cape Adare and Ross Sea) has been noted by, for example, Hoskins and Hodges (2005) as the termination area of storms that spiral in towards Antarctica from the southern Indian Ocean and south of Australia.

The corresponding EKE values for the fully coupled versions of CESM1, 1x1_v1.1, 1x1_v1.3, 0.25x1_v1.3, and 0.25x0.1_v1.1, are shown in Fig. 1a through d, respectively. All model versions simulate midlatitude storm track EKE maxima in the southeast Pacific near 45˚S, and in the southern Atlantic/Indian Oceans near 55˚S in agreement with the observations as represented by the ERA-Interim reanalysis (Fig. 1e). For the one degree CESM1 versions,

the improved physics in 1x1_v1.3 (Fig. 1b) compared to 1x1_v1.1 (Fig. 1a) show increases in storm track strength in the south Atlantic of about 15% (maxima greater than 17 m^2 sec^{-2} in 1x1_v1.3 compared to about 16 m^2 sec^{-2} in 1x1_v1.1). However, these simulated EKE values in the 1˚ versions are weaker than the reanalysis values of around 19 m^2 sec^{-2} in that region in Fig. 1e by about 20%.

With increased resolution in the atmosphere in 0.25x1_v1.3 (Fig. 1c), as could be expected from the discussion above, the storm track intensity increases by about 20% compared to the 1˚ versions in Fig. 1a,b, in closer agreement to the reanalysis (Fig. 1e). However, with that same resolution in the atmosphere but with the older physics, and in spite of increased resolution in the ocean to 0.1˚, in 0.25x0.1_v1.1 the storm tracks weaken by about 15% and shift southward (Fig. 1d) compared to the CESM1.3 with improved physics in 0.25x1_v1.3 (Fig. 1c) and the reanalysis (Fig. 1e). A notable feature of the 0.25° coupled simulations and the 0.25° AMIP simulations is that they show the local maximum off Antarctica at around 180° (Figs. 1c,d,g,h), consistent with ERA interim, but not seen in the 1° models (Fig. 1a,b,f). This is consistent with previous research that has shown higher resolution in the atmosphere can better resolve storm dynamics and thus produce better storm tracks (e.g. Roberts et al., 2018). Additionally, the more highly resolved topography of the Antarctic coastline contributes to better simulation of the storms as they near Antarctica (Uotila et al., 2009).

Though we focus here on results for the Southern Hemisphere, these storm track responses as a function of model version can be generalized to the Northern Hemisphere (Fig. S1). Subsampling the large ensemble in Fig. 1a by randomly selecting three members produces similar results in Fig. S2b to that in Fig. 1a (and repeated in Fig. S2a) with maximum EKE

differences of only about 3% which are well below the differences of 10-20% shown for other model versions.

It has been noted that the equator-to-pole midtropospheric temperature gradient is a measure of the broadscale baroclinicity of the atmosphere as it is required to move excess heat from the tropics poleward in part by midlatitude eddies (e.g. Harvey et al., 2014). Thus, the equator-to-pole temperature gradient is related to changes in storm tracks, as represented by EKE in Fig. 1. The meridional temperature gradient in Fig. 2a shows the differences of annual mean 500 hPa temperatures at 70-90˚S minus 0-20˚S. Annual means are shown in Fig. 2 since the manifestations of JJA storm tracks receive contributions from processes throughout the year that effect seasonal SSTs and corresponding mid-tropospheric temperature gradients (e.g. van Loon, 1967; seasonal values are qualitatively similar, not shown). Average values of this difference are about 33˚C for the reanalysis. Both the 1x1_v1.1 and 1x1_v1.3 have mean values near 33.1˚C that is within the error bars of the reanalysis. The small increases in storm track intensity in 1x1_v1.3 compared to 1x1_v1.1 in Fig. 1a are likely related to either sampling or the dynamical core (SE in the former, FV in the latter). Either way, both are considerably weaker than the reanalysis in spite of having comparable meridional temperature gradients. As noted above, the 0.25x1_v1.3 has larger values of EKE closer to observations than either of the 1˚ versions (1x1_v1.1 or 1x1_v1.3). This is likely due to either the increased atmospheric model resolution in the former, or to the increased meridional temperature gradient with a value in the former of about 33.9˚C compared to around 33.1˚C in the latter (Fig. 2a). However, the weakened storm tracks in 0.25x0.1_v1.1 compared to 0.25x1_v1.3 (Fig. 1c,d) are consistent with the weaker meridional temperature gradient in the former compared to the latter (32.1˚C vs 33.9˚C, respectively). The weakening of the storm tracks in 0.25x0.1_v1.1 appears to have a strong contribution

from changes in meridional temperature gradient that could relate to the different physics formulations. Thus there are two things going on in these simulations. First the meridional temperature gradient can contribute to storm track strength, all else being equal. Second, the atmospheric model resolution is changing, and higher resolution better resolves storm dynamics and can produce increases in EKE. Therefore, the 1x1 versions have a well-simulated meridional temperature gradient but do not have high enough atmospheric resolution to produce a good simulation of EKE. But the 0.25˚ versions have contrasting meridional temperature gradients (with 1.3 better than 1.1) such that those temperature gradients are making the major contribution to the changes in EKE.

Another possibility is that explicit ocean eddies in in 0.25x0.1_v1.1 versus parameterized ocean eddies in 0.25x1_v1.3 could be playing a role. However, Small et al., (2018) note that versions of CESM1 with a 0.1˚ ocean compared to a 1˚ ocean, both coupled to the same 0.25 ˚ atmosphere with the same physics, produces somewhat greater meridional SST gradients in the Southern Ocean and increased baroclinicity (their Figs. 4, 9, and 12). Since the opposite is occurring here, something else is overwhelming the tendency that could be expected for a higher resolution ocean to contribute to increased baroclinicity and more intense atmospheric eddies over the Southern Ocean.

b. The role of physics and coupling

As noted above, the atmospheric model in 0.25x0.1_v1.1 has a previous version of the physics dating from CESM1.1. There are lower SSTs in the midlatitude Southern Ocean where the SST differential between these two 0.25˚ versions over 40-50˚S is around 1˚C (Fig. 2b), while the differential is negligible near 20˚S. This can be traced to the improvements in physics in the CAM5 added in 0.25x1_v1.3 (CESM1.3 beta 17) that produce more low

clouds over the Southern Ocean (Fig. 2c). For example at 50˚S, there are low cloud fractions of about 0.72 in 0.25x1_v1.3 and only 0.66 in 0.25x0.1_v1.1. This large low cloud contrast contributes to changes in the surface energy balance and an increased meridional SST gradient in 0.25x1_v1.3. This can be attributed in part to the larger low cloud fraction in 0.25x1_v1.3 over the Southern Ocean near 50˚S that results in less incoming solar (111.4 W m^{-2}) compared to 0.25x0.1_v1.1 (119.1 Wm^{-2}) in Table 1. The net surface energy flux near 50˚S is about 4 W m^{-2} less in 0.25x1_v1.3 compared to 0.25x0.1_v1.1. Thus the improvement in physics in 0.25x1_v1.3 increases midlatitude low clouds, decreases incoming solar radiation at the surface, decreases midlatitude SSTs, and contributes to an increased meridional temperature gradient, and stronger storm tracks in 0.25x1_v1.3 compared to 0.25x0.1_v1.1.

This change in physics is also evident in comparing the 1x1_v1.1 with 1x1_v1.3. In the former there are decreased low clouds, increased net solar at the surface, and increased midlatitude SSTs compared to the latter. It is likely that linkages to cloud and SST changes are contributing to the slightly stronger storm track in 1x1_v1.3 (Fig. 1b) compared to 1x1_v1.1 (Fig. 1a). The changes in SST gradient are not reflected in the midtropospheric temperature gradient and the storm track simulations, though both are weaker than reanalysis, and are more comparable than the 0.25˚ atmospheric model versions. The exact reasons for these features in the vertical are beyond the scope of the present paper but likely involve differences in vertical mixing and boundary layer processes in the 1˚ versions compared to the 0.25˚ versions.

Another interesting aspect of these differences in atmospheric model physics is that the changes in low clouds and altered storm tracks show up most strongly in the coupled model

versions. In AMIP runs with the two 0.25˚ atmospheric model versions (amip_0.25d_v1.1 and amip_0.25d_v1.3), the low cloud simulations are nearly the same in association with identical SST specifications in the AMIP configuration, with somewhat greater low cloud amounts in the midlatitudes in amip_1d_v1.3 (Fig. S5). There is only a marginal increase in storm track strength in the AMIP versions of CESM1.3 going from 1˚ to 0.25˚ (Fig. 1f,g) with a slight weakening of midtropospheric meridional temperature gradient (Fig. S4). This is in contrast with the nearly 20% increase in storm track strength in the coupled versions of those models (Fig. 1b,c) and the much stronger meridional temperature gradient at higher resolution (Fig. 2a). Similarly, the AMIP version of 0.25x0.1_v1.1 shows a comparable storm track strength compared to the AMIP version of 0.25x1_v1.3 (Fig. 1g,h) with similar meridional temperature gradients (Fig. S4). But there is a considerable weakening of storm tracks and meridional temperature gradients comparing the two 0.25˚ coupled versions (Fig. 1c,d; and Fig. 2a, respectively). This points to the importance of air-sea coupling in the physics changes that affect the simulation of low clouds and their impacts on surface energy balance, meridional temperature gradient, and storm tracks. These connections between meridional SST gradient, low level winds, and baroclinicity over a large area of the Southern Ocean were demonstrated by Small et al. (2018, their Figs. 4, 6, and 12).

Some previous studies (e.g. Sheldon et al., 2017; Small, et al., 2018) hypothesize that, in addition to the meridional SST gradient, the base state SST also can have a significant impact on the storm track simulation through latent heat flux from the surface. Based on Fig. 2b, it was noted earlier that 0.25x0.1_v1.1 with the older physics has warmer midlatitude SSTs by about 1˚C compared to 0.25x1_v1.3. Yet the former has considerably weaker storm tracks than the latter, indicating that the effects of meridional temperature gradient (weaker in

the former compared to the latter, Fig. 2a) contribute more to storm track strength than background base state SSTs in these simulations.

4. Summary

The previous physics in the CAM5 version in 0.25x0.1_v1.1 produce fewer low clouds, allowing sunlight to heat the surface more in the midlatitudes than the tropics, thus weakening the meridional temperature gradient, reducing baroclinicity, and producing lower values of EKE and a degraded storm track simulation compared to 0.25x1_v1.3 with improved physics. These changes in atmospheric model physics outweigh base state values of SST and changes in ocean model resolution. The implications of this result are that simply improving resolution in atmosphere or ocean does not guarantee a better simulation of climate system dynamics. Instead, it is the combination of improved physics and improved resolution in the atmosphere that produce a better simulation of Southern Hemisphere storm tracks in 0.25x1_v1.3 represented by 850 hPa EKE.

Acknowledgements

Portions of this study were supported by the Regional and Global Model Analysis (RGMA) component of the Earth and Environmental System Modeling Program of the U.S. Department of Energy's Office of Biological & Environmental Research (BER) via National Science Foundation IA 1844590, This work also was supported by the National Center for Atmospheric Research, which is a major facility sponsored by the National Science Foundation under Cooperative Agreement No. 1852977, and by the Australian Research Council Centre of Excellence for Climate Extremes (grant CE170100023). The CESM project is supported primarily by the National Science Foundation. Most figures were created

using NCAR Command Language (NCL) version 6.5.0. This research was undertaken with the assistance of resources and services from the Climate Simulation Laboratory within NCAR's Computational and Information Systems Laboratory (doi:10.5065/D6RX99HX), sponsored by the National Science Foundation and other agencies. An award of computer time was provided by the Innovative and Novel Computational Impact on Theory and Experiment (INCITE) program. This research used resources of the Argonne Leadership Computing Facility, which is a DOE Office of Science User Facility supported under Contract DE-AC02-06CH11357. This research is also part of the Blue Waters sustained-petascale computing project, which is supported by the National Science Foundation (awards OCI-0725070 and ACI-1238993) and the state of Illinois. Blue Waters is a joint effort of the University of Illinois at Urbana-Champaign and its National Center for Supercomputing Applications. This work is also part of the "High Resolution Earth System Modeling Using Blue Waters Capabilities" PRAC allocation support by the National Science Foundation (award number ACI-1516624).

Data availability: The relevant model data are available from https://doi.org/10.26024/v3at-xa25.

ERA-Interim reanalysis are available from https://www.ecmwf.int/en/forecasts/datasets/reanalysis-datasets/era-interim. Observed SSTs are from https://climatedataguide.ucar.edu/climate-data/merged-hadley-noaaoi-sea-surface-temperature-sea-ice-concentration-hurrell-et-al-2008.

References

Adcroft, A., C. Hill and J. Marshall (1997), Representation of topography by shaved cells in a height coordinate ocean model. *Mon. Wea. Rev*., **125**, 2293-2315.

Bacmeister, J. T., M. F. Wehner, R. B. Neale, A. Gettelman, C. Hannay, P. H. Lauritzen, J. M. Caron and J. E. Truesdale (2014), Exploratory High-Resolution Climate Simulations using the Community Atmosphere Model (CAM), *J. Clim.*, *27*, 3073–3099.

Baker, A.H., et al. (2015), A new ensemble-based consistency test for the Community Earth System Model (phCECTv1.0), *Geosci. Model Dev*., **8**, 2829–2840, www.geosci-model-dev.net/8/2829/2015/doi:10.5194/gmd-8-2829-2015.

Bony, S., B. Stevens, D.M.W. Frierson, C. Jakob, M. Kageyama, R/ Pincus, M.J. Webb, (2015), Clouds, circulation and climate sensitivity. *Nature Geoscience***, 8**, 261–268. https://doi.org/10.1038/NGEO2398

Brady, E.C., et al. (2019), The connected isotopic water cycle in the Community Earth System Model version 1, *JAMES*, **11**, doi:10.1029/2019MS001663.

Ceppi, P., and D.L. Hartmann, D. L. (2015), Connections between clouds, radiation, and midlatitude dynamics: A review. *Current Climate Change Reports*, 1, 94. https://doi.org/10.1007/s40641-015-0010-x.

Danabasoglu, G., S. C. Bates, B. P. Briegleb, S. R. Jayne, M. Jochum, W. G. Large, S. Peacock, and S. G. Yeager, (2011), The CCSM4 ocean component. *J. Climate*, **25**, 1361–1389.

Dennis, J, J. Edwards, K. J. Evans, O. N. Guba, P. H. Lauritzen, A. Mirin, A. St.-Cyr, M. Taylor and P. H. Worley (2012), CAM-SE: A scalable spectral element dynamical core for the community atmosphere model, *International Journal for High Performance Computing Applications,* **26**, 74-89, doi: 10.1177/1094342011428142.

Gent, P. R., and J. C. McWilliams, (1990), Isopycnal mixing in ocean circulation models. *J Phys. Oceanogr.* **20**, 150-155.

Grise, K. M., and L.M. Polvani,. (2014), Southern Hemisphere cloud-dynamics biases in CMIP5 models and their implications for climate projections. *J. Clim.*, **27**, 6074–6092. https://doi.org/10.1175/JCLI-D-14-00113.1

Harvey, B.J., L.C. Shaffrey, and T.J. Woolings, (2014), Equator-to-pole temperature differences and the extra-tropical storm track responses of the CMIP5 climate models. *Clim. Dyn*., **43**, 1171—1182, doi:10.1007/s00382-013-1883-9.

Hertwig, E., et al. (2015), Effect of horizontal resolution on ECHAM6-AMIP performance, *Clim. Dyn*, **45**, 185—211, doi:10.1007/s00382-014-2396-x.

Hoskins, B.J., and K.I. Hodges (2005), A new perspective on Southern hemisphere storm tracks. *J Clim*, **18**, 4108-4129.

Hunke, E. C., and W. H. Lipscomb, (2008), CICE: the Los Alamos sea ice model user's manual, version 4. Los Alamos National Laboratory Tech. Rep. LA-CC-06-012.

Hurrell, J. W., J. J. Hack, D. Shea, J. M. Caron, and J. Rosinski, (2008), A new sea surface temperature and sea ice boundary dataset for the Community Atmosphere Model. *J. Climate*, **21**, 5145–5153, doi:10.1175/2008JCLI2292.1.

Hurrell, J. W., and Coauthors, (2013), The Community Earth System Model: A Framework for Collaborative Research. *Bull. Amer. Meteor. Soc.*, **94**, 1339–1360.

Inatsu N, and B.J. Hoskins, (2004), The zonal asymmetry of Southern hemisphere winter storm track. *J Clim.*, **17**, 4882-4892

Kay, J. E., B. R. Hillman, S. A. Klein, Y. Zhang, B. Meideiros, R. Pincus, A. Gettelman, B. Eaton, J. Boyle, R. Marchand and T. P. Ackerman, (2012), Exposing global cloud biases in the Community Atmosphere Model (CAM) using satellite observations and their corresponding instrument simulators. *J. Clim.*, **25**, 5190-5207.

Kay, J. E., et al. (2015), The Community Earth System Model (CESM) Large Ensemble Project: A Community Resource for Studying Climate Change in the Presence of Internal Climate Variability. *Bull. Am. Meteorol. Soc.*, **96**, 1333–1349, doi:10.1175/BAMS-D-13-00255.1.

Kirtman, B.P., C.C. Bitz, W. Collins, J. Dennis, N. Hearn, J.L. Kinter, R. Loft, C. Rosset, L. Siqueira, C. Stan, R. Tomas and M. Vertenstein (2012), Impact of ocean model resolution on CCSM climate simulations, *Clim. Dyn.*, **39**, 1303-1328.

Lauritzen, P.H., et al. (2019), NCAR release of CAM-SE in CESM2.0: A reformulation of the spectral element dynamical core in dry-mass vertical coordinates with comprehensive treatment of condensates and energy. *JAMES*, https://doi.org/10.1029/2017MS001257.

Lawrence, D. M., K. W. Oleson, M. G. Flanner, P. E. Thornton, S. C. Swenson, P. J. Lawrence, X. Zeng, Z.-L. Yang, S. Levis, K. Sakaguchi, G. B. Bonan and A. G. Slater, (2011), Parameterization improvements and functional and structural advances in version 4 of the Community Land Model, *J. Adv. Model. Earth Syst.*, **3**, Art. 2011MS000045.

Maloney, E.D. (2009), The moist static energy budget of a composite tropical intraseasonal oscillation in a climate model. *J. Clim*., **22**, 711—729, doi:10.1175/2008jcli2542.1.

McClean, J. L., and 14 co-authors, (2011), A prototype two-decade fully-coupled fine resolution CCSM simulation. *Ocean Modelling*, **39**, 10-30.

Medeiros, B., D.L. Williamson, C. Hannay, and J.G. Olson, (2012), Southeast Pacific stratocumulus in the Community Atmosphere Model. *J. Clim*., **25**, 6175—6192, doi:10.1175/JCLI-D-11-00503.1.

Meehl, G.A., W.M. Washington, J.M. Arblaster, A. Hu, H. Teng, C. Tebaldi, B. Sanderson, J-F Lamarque, Andrew Conley, W.G. Strand, and J.B. White III, (2012), Climate system

response to external forcings and climate change projections in CCSM4, *J. Climate*, **25**, 3661-3683

Meehl G.A., W.M. Washington, J.M. Arblaster, A. Hu, H. Teng, J.E. Kay, A. Gettelman, D.M. Lawrence, B.M. Sanderson, W.G. Strand, (2013), Climate change projections in CESM1(CAM5), *J. Climate*, **26**, doi:10.1175/JCLI-D-12-00572.1

Murphy, B.F., P. Pettre, and I. Simmonds (2002), Effects of changing baroclincity on the southern Hemisphere extratropical circulation. *Q.J.R.Meteorol. Soc*., **128**, 1807—1826.

Nakamura, H/, and A. Shimpo (2004), Seasonal variations in the Southern Hemisphere storm tracks and jet streams as revealed by a reanalysis dataset. *J Clim*, **17**, 1828-1842.

Park, S., C. S. Bretherton, and P. J. Rasch, (2014), Integrating cloud processes in the Community Atmosphere Model, Version 5. *J. Clim.*, **27**, 6821-6856.

Roberts, M.J., et al. (2018), The benefits of global high resolution for climate simulation. *Bull. Amer. Meteorol. Soc*., **99**, 2341—2359, doi:10.1175/BAMS-D-15-00320.1.

Shaffrey, L.C., and co-authors (2009), U.K. HiGEM: The new U.K. high-resolution global environment model—model description and basic evaluation. *J. Climate*, **22**, 1861—1896, DOI: 10.1175/2008JCLI2508.1.

Sheldon, L., Czaja, A., Vannière, B., Morcrette, C., Sohet, B., Casado, M., & Smith, D. (2017), A 'warm path'for Gulf Stream–troposphere interactions. *Tellus A: Dynamic Meteorology and Oceanography,* **69(1)**, 1299397.

Small, R. J., et al. (2014), A new synoptic scale resolving global climate simulation using the Community Earth System Model, *J. Adv. Model. Earth Syst*., **6**, 1065–1094, doi:10.1002/2014MS000363.

Small, R.J., R. Msadek, Y.-O. Kwon, J.F. Booth, and C. Zarzycki (2018), Atmosphere surface storm track response to resolved ocean mesoscale in two sets of global climate model experiments. *Clim. Dyn.*, https://doi.org/10.1007/s00382-018-4237-9.

Smith, R. D., et al. (2010), The Parallel Ocean Program (POP) reference manual. Los Alamos National Laboratory Tech. Rep. LAUR-10-01853.

Tilmes, S, et al., (2015), Description and evaluation of tropospheric chemistry and aerosols in the Community Earth System Model (CESM1.2). *Geoscientific Model Development*, **8**. 1395 - 1426. ISSN 1991-959X.

Trenberth KE (1991), Storm tracks in the Southern Hemisphere. *J Atmos Sci*, **48**, 2159-2178.

Uotila, P., A.B. Pezza, J.J. Cassano, I. Keay, and A.H. Lynch, (2009), A comparison of low pressure system statistics derived from a high-resolution NWP output and three reanalysis products over the Southern Ocean. *J. Geophys. R*es., **114**, D17105, doi:10.1029/2008JD011583.

Zarzycki, C.M., et al. (2016), Impact of surface coupling grids on tropical cyclone extremes in high-resolution atmospheric simulations. *Geosci. Model. Dev.*, **9,** 779—788, doi:10.5194/gmd-9-779-2016.

Table 1 Summary of experiments and surface energy balance over the ocean at 50°S

No. members	Experiments	Model Version	Air-Res	Ocean-Res	Period
Coupled Model simulations					
142	1x1_v1.1	CESM-LENS-1.1	1°	1°	1979-2005
23	1x1_v1.3	CESM1.3-beta17	1°	1°	1979-2005
3	0.25x1_v1.3	CESM1.3-beta17	0.25°	1°	1979-2005
41	0.25x0.1_v1.1	CESM1.1-ASD	0.25°	0.1°	Present Day (monthly data 27 years, daily data 10 years)
Atmosphere-only Model simulations (AMIP)					
5	amip_1d_v1.3	CESM1.3-beta17	1°	—	1979-2005 1
6	amip_0.25d_v1.3	CESM1.3-beta17	0.25°	—	1979-2005 1
71	amip_0.25d_v1.1	CESM1.1-ASD	0.25°	—	1979-2005

Surface Energy Balance over the ocean at 50°S

Experiments	Solar flux	Longwave flux	Sensible Heat flux	Latent Heat flux	Net
1x1_v1.1	117.64	40.87	10.71	54.05	12.01↓
1x1_v1.3	115.01	38.49	12.50	53.51	10.51↓
0.25x1_v1.3	111.40	36.58	9.87	52.51	12.44↓
0.25x0.1_v1.1	119.06	39.96	8.40	54.29	16.41↓

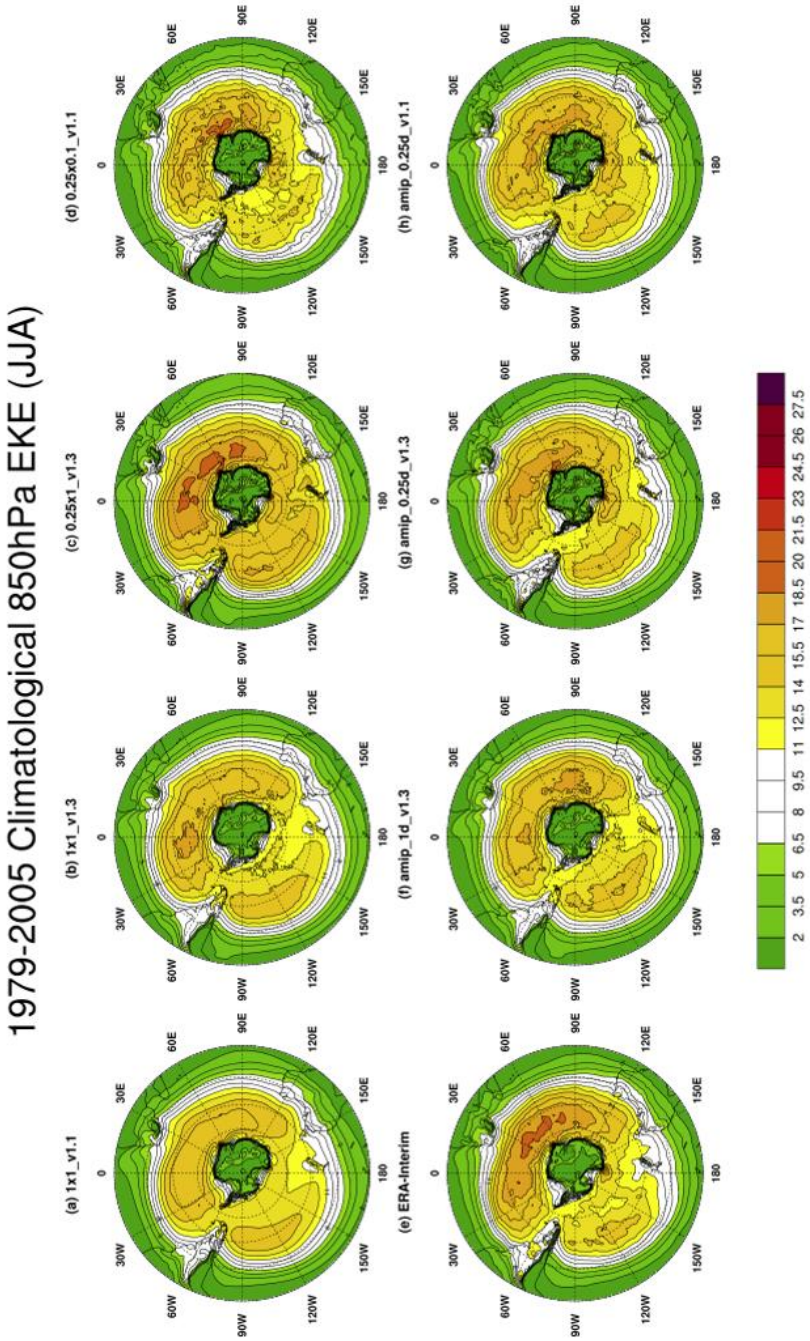

Figure 1: Climatological JJA 850hPa Southern Hemisphere eddy kinetic energy (EKE), m^2 sec^{-2}, representing storm tracks for (a) CESM1.1 (1x1_v1.1), averaged over 1979-2005; (b) CESM1.3 (1x1_v1.3), averaged over 1979-2005; (c) CESM1.3 (0.25x1_v1.3), averaged over 1979-2005; (d) CESM1.1 (0.25x0.1_v1.1), using year-2000 radiative forcings (27 years).; e) ERA-Interim averaged over 1979-2005; f) same as (b) except for the AMIP version (amip_1d_v1.3); g) same as (c) except for the AMIP version (amip_0.25d_v1.3); h) same as (d) except for the AMIP version (amip_0.25d_v1.1). Dotted latitude lines are plotted every 15˚, at 15˚S, 30˚S, 45˚S, 60˚S, and 75˚S.

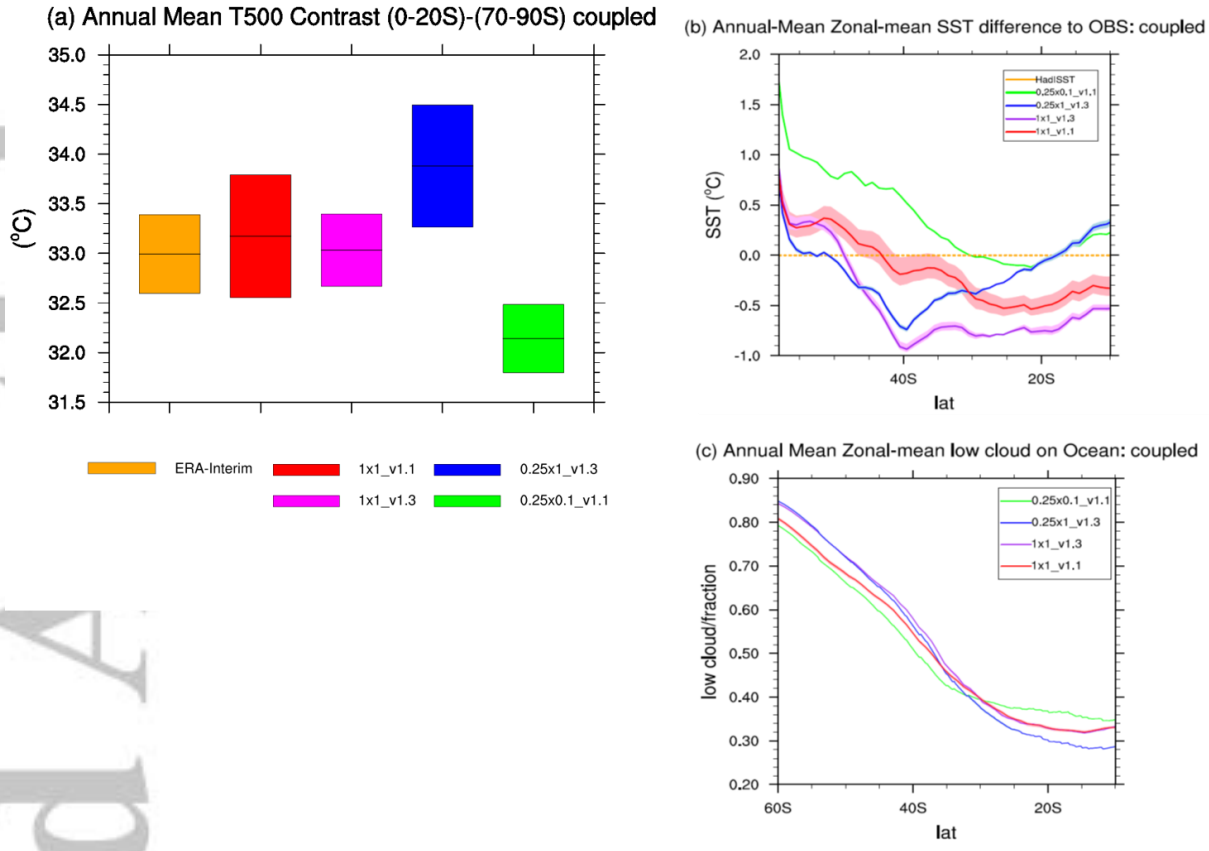

Figure 2: Climatological annual zonal-mean a) 500 hPa meridional temperature difference, lower latitudes (0-20˚S) minus higher latitudes (70-90˚S), ˚C, ERA-Interim and CESM coupled simulations noted by bar colors at bottom of panel; for each simulation, the black reference line is the average, with the top and bottom of each bar the +/- one standard deviation values multiplied by

$\sqrt{n}$ where n is the number of ensembles in the respective model simulations

to make the spread more comparable across the different model versions with different numbers of ensemble members; b) zonal mean SSTs from 60˚S to 10˚S, ˚C, model values computed in reference to the observations, model color key in upper right, shading indicates range across the ensemble; c) same as (b) except for low cloud fraction (shading across ensemble range is plotted but ensemble range is small).